Improving the performance of si-based li-ion battery anodes by utilizing phosphorene encapsulation

Peng, Bo; Xu, Yao Lin; Mulder, Fokko M.

DOI
10.3866/PKU.WHXB201705244

Publication date
2017

Document Version
Accepted author manuscript

Published in
Wuli Huaxue Xuebao/ Acta Physico - Chimica Sinica

物理化学学报(*Wuli Huaxue Xuebao*)
Month *Acta Phys. -Chim. Sin.* **2017,** *33* (X), 0001−0009 0001

[Communication] doi: 10.3866/PKU.WHXB2017xxxxx www.whxb.pku.edu.cn

磷烯包覆的高性能硅基锂离子电池负极材料

彭 勃[1,2] 徐耀林[2] Fokko M. Mulder[2,*]

([1]中国人民大学物理系，北京 100872；[2] Materials for Energy Conversion and Storage (MECS), Department of Chemical Engineering, Faculty of Applied Science, Delft University of Technology, Delft 2629 HZ, The Netherlands)

摘要：硅基锂离子负极材料在脱嵌锂离子的过程中显著的体积效应导致活性材料的粉化、固体电解质介面膜 (SEI)的持续生长和电接触的丧失并最终导致电池的失效。本文报道了一种新型的磷烯（单层黑磷）包覆法来提升硅基负极材料的电化学性能。微量（1%）的磷烯包覆有效抑制了被包覆硅颗粒的体积膨胀和SEI生长等问题，并保持了其电极结构在持续充放电循环中的完整性，从而提升了其库伦效率、容量以及循环稳定性。这是首次利用磷烯包覆法来提升硅基锂离子电池负极材料电化学性能的报道，而且也展现了此工艺在其他具有显著体积效应的电池材料中具有应用前景。

关键词：磷烯；锂离子电池；负极材料；硅

中图分类号：O646

Improving the performance of si-based li-ion battery anodes by utilizing phosphorene encapsulation

PENG Bo[1,2] XU Yao-Lin[2] MULDER Fokko M.[2,*]

([1]*Department of Physics, Renmin University of China, Beijing 100872, China*; [2]*Materials for Energy Conversion and Storage (MECS), Department of Chemical Engineering, Faculty of Applied Science, Delft University of Technology, Delft 2629 HZ, The Netherlands*)

Abstract: Si based anode materials in Li ion batteries suffer from severe volume expansion/contraction during repetitive discharge/charge, which results in the pulverization of active materials, continuous growth of solid electrolyte interface (SEI) and loss of electrical conduction, and eventually, the battery failure. This work presents a novel and facile approach of low-content phosphorene (single layer black phosphorus) encapsulation on silicon particles as an effective method to improve the electrochemical performance of Si based Li ion battery anodes. The incorporation of a low amount of phosphorene (1%, mass fraction) in the Si anodes appeared to effectively suppress the detrimental effects of volume expansion and SEI growth. It appears to maintain the structural integrity of the electrode during repetitive discharge/charge, resulting in an enhanced Coulombic efficiency, capacity retention and cycling stability for Li ion storage. This is the first introduction of phosphorene encapsulation in Si based anodes with the aim to improve the cycling performance in Li ion batteries and may also show promise for the application in other high energy density batteries materials with substantial volume changes.

Key Words: Phosphorene; Li ion battery; Anode materials; Silicon;

Received: date; Revised: date; Published online: date.

*Corresponding author. Email: F.M.Mulder@tudelft.nl; Tel: +31-15-2785037

This work was financially supported by Chinese Scholarship Council (CSC) and the "A green Deal in Energy Materials" (ADEM) program.
该研究由中国留学基金委和荷兰经济事务部绿色能源材料项目资助。

1 Introduction

In the recent years research on Li ion batteries has intensified due to the extremely high demand in large scale and high energy density energy storage devices all over the world, and Li ion batteries are playing a dominant role in the market of rechargeable batteries[1–4].

Si based materials have been intensively studied the anodes for Li ion batteries due to its highest theoretical capacity for Li ion storage (4200 $mAh \cdot g^{-1}$ for $Li_{4.4}Si$)[5–9].However, a large amount of volume expansion (> 300%) takes plac e when Li ions are inserted into the Si structure, while the structure collapses upon the extraction of Li ions which leads to the irreversible and adverse material pulverization, resulting in the loss of electrical conduction between the grains of the active materials[7,9]. Moreover, an irreversible solid electrolyte interface (SEI) grows continuously due to the decomposition of electrolyte solvents and their reactions with the active materials and causes the loss of active materials[7,10].

Various methods have been applied to address these issues. Surface encapsulation with nanostructured carbonaceous materials such as graphene has been reported to result in positive effects in suppressing the volume change upon Li ion uptake and in maintaining the electrode structural integrity, which enhances the cycling stability during discharge/charge[11–15]. Exhibiting a low band gap of 0.3 − 2 eV[16,17] and a similar layered structure as graphene, phosphorene (single layer black phosphorus) has recently attracted much research interest in semiconductor science and energy storage devices including Li ion batteries due to its 2D structure, high charge carrier mobility and low band gap[18–21]. Zhang *et al*.[20] reported that Li diffusion in phosphorene is about 10^4 times faster than in graphene which enables a remarkable high rate performance. Therefore the incorporation of phosphorene in Si anodes may lead to similar effects as graphene and may allow even facilitated Li ion uptake when compared to graphene.

Moreover, phosphorus doping within the Si crystal lattice has also been proven to be an effective method to improve the electrochemical performance of Si anodes in Li ion batteries[22–26]. The incorporation of phosphorus leads to the suppression of volume expansion, enhancement in the electronic conductivity and the improved structural stability of the electrodes, and thus the cycling stability is improved.

Inspired by the methods of surface encapsulation and phosphorus doping, in this work, we have developed a Si anode that combines the above approaches. Ball milled nanoscale Si particles were encapsulated by mechanochemically synthesized and liquid-phase exfoliated phosphorene and the amount of phosphorene present next to Si is kept low (1%, mass fraction) with the rationale that it should serve as a thin coating only on Si particles and their aggregates. The phosphorene encapsulated Si particles exhibits a significantly improved capacity retention and cycling stability for reversible Li ion storage compared to bare Si by suppressing the volume swelling and SEI growth during discharge/charge.

2 Experimental and computational section

2.1 Synthesis of black phosphorus

Black phosphorus was synthesized *via* a mechanochemical method. Specifically commercial red phosphorus (Alfa Aesar, 99%) was ball milled at 400 $r \cdot min^{-1}$ for 70 h with a ball-to-powder mass ratio of 100:1 under argon atmosphere using a Fritsch Planetary Mono Mill PULVERISETTE 6, during which red phosphorus was mechanochemically transformed to black phosphorus.

2.2 Synthesis of phosphorene

Phosphorene was produced via a liquid-phase exfoliation approach which was adopted from the previously reports[27,28]. The as-synthesized black phosphorus was dispersed in *N*-methyl-2-pyrrolidone (NMP) in a concentration of 0.5 $mg \cdot ml^{-1}$ and sonicated in a ultrasonic bath for 60 min, right after which it was centrifuged using an Eppendorf 5804 centrifuge for 60 min operating at 4000 $r \cdot min^{-1}$. This sonication-centrifugation treatment was repeated for 5 times. Subsequently, the supernatant fluid was decanted. The black phosphorus sediments could be reusable in the phosphorene production. This method resulted in a phosphorene yield of 17 $\mu g \cdot ml^{-1}$ in NMP according to the previous report[21].

2.3 Synthesis of phosphorene encapsulated Si

Phosphorene encapsulated Si (*p*-Si) was prepared by the following procedures: Firstly, silicon powder (Aldrich, −325 mesh, 99%) was ball milled for 10 h at 200 $r \cdot min^{-1}$ with a ball-to-powder ratio of 50:1 in mass. Then, the ball milled Si particles were dispersed in NMP and sonicated in an ultrasonic bath for 5 h to reduce the aggregates formed in ball milling. Subsequently the phosphorene saturated NMP solution was added (phosphorene : Si = 1 : 99 in mass) and uniformly mixed with the assistance of magnetic stirring. Finally, the well-mixed liquid was heated at 150 ℃ under argon environment to evaporate the solvent during which the solution was stirred continuously. The *p*-Si sample was obtained when NMP was completely evaporated.

2.4 Sample characterization

X-ray diffraction (XRD) patterns were acquired using a PANalytical X'Pert Pro PW3040/60 diffractometer that uses a Cu K_α source working at 45 kV and 40 mA. Raman spectroscopy was performed with a Thermo Scientific Nicolet Almega XR Dispersive Raman Spectrometer. Scanning electron microscopy (SEM) was carried out with a JEOL JSM 6010F scanning electron microscope which operates at an accelerating voltage of 5 kV; SEM based Energy-dispersive X-ray spectroscopy (EDX) was conducted at an accelerating voltage of 20 kV. X-ray photoelectron spectroscopy (XPS) spectra were obtained using a K_α Thermo Fisher Scientific spectrometer.

2.5 Electrode preparation

The working electrodes were prepared with a slurry based

method. Bare Si/*p*-Si powders, super P carbon black and sodium carboxymethyl cellulose (NaCMC) binder were mixed with a mass ratio of 8:1:1 in deionized water and ball milled for 2 h at 200 r·min^{-1} to obtain a homogeneous slurry. Subsequently the slurry was cast onto a piece of Cu foil current collector (12.5 μm, Goodfellow) using a doctor blade. After drying in a vacuum operating at 70 ℃ overnight, the electrodes were mechanically pressed and punched into circular pieces for the final battery assembly. The mass loading of Si/*p*-Si on the electrodes was about 1.0 mg·cm^{-2}.

2.5 Electrochemistry measurement

Bare Si and *p*-Si anodes based Li-ion coin cells (CR 2032) were assembled in an argon atmosphere glove box. Li metal was applied as the counter electrode and borosilicate glass fiber (Whatman) was used as the separator. The working electrolyte was 1 mol·L^{-1} $LiPF_6$ dissolved in ethylene carbonate (EC) and diethyl carbonate (DEC) (EC/DEC = 1:1 in voulme) with the addition of 10% fluoroethylene carbonate (FEC). The electrochemical properties were characterized using a Maccor 4600 battery cycler and the voltage range for discharge/charge was limited to 0.01 – 1 V *vs.* Li/Li$^+$.

3 Results and discussion

SEM images (**Fig.1(a, b)**) shows that pristine red phosphorus appears as big particles mostly on tens of microns scale; after ball milling, the particle size is much reduced and the as-synthesized black phosphorus appears to be submicro-/nanosized particles and agglomerations of these small particles.

In the XRD pattern of the as-synthesized black phosphorus (**Fig.1c**), all peaks observed can be assigned to characteristic Bragg diffraction peaks of black phosphorus (Pearson's Crystal Data (PCD) #1639521, space group: *Cmce*) indicating the formation of black phosphorus.

The Raman spectrum of the pristine red phosphorus (**Fig.1d**) is consistent with that of the amorphous red phosphorus in previous reports[29–32]. The ball milled sample shows three distinct peaks at 358, 433, 461 cm^{-1} corresponding to the A_{1g}, B_{2g} and A_{2g} vibrational Raman modes, respectively, of black phosphorus[30,33,34]. This is consistent with the XRD results indicating the mechanochemical transformation from red phosphorus to black phosphorus.

The particle size of Si has been significantly reduced during the high energy ball milling, which is evidenced by the obvious peak broadening of the XRD peaks of crystalline Si (**Fig.2a**). Weak peaks corresponding to SiO_2 can also be recognized from the XRD patterns which corresponds to the unavoidable surface oxidation of Si particles when the ball milled Si sample was exposed to air[35,36].The SEM image (**Fig.2b**) shows that ball milled Si consists of submicro-/nanosized particles and agglomerations. SEM-EDX element mapping on the *p*-Si sample (**Fig.2(c–e)**)

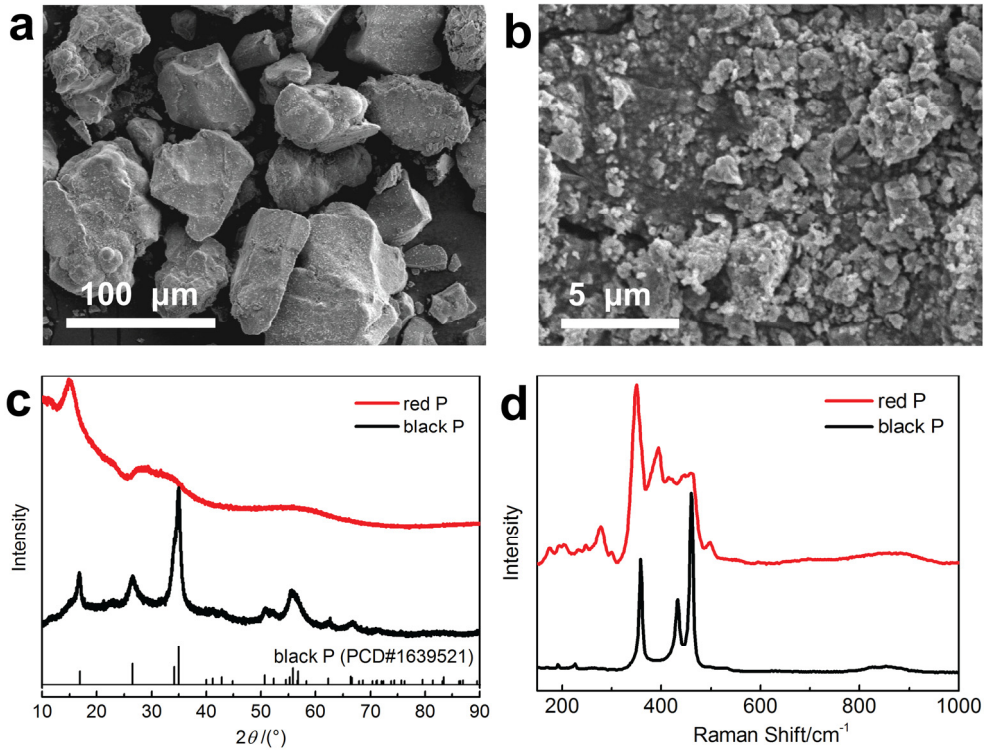

Fig.1 Characterization on the pristine red phosphorus and as-synthesized black phosphorus.

(a), SEM image of the pristine red phosphorus; (b), SEM image of the as-synthesized black phosphorus; (c), XRD patterns and (d), Raman spectra. (reference XRD pattern of black phosphorus: Pearson's Crystal Data (PCD) entry No. 1639521)

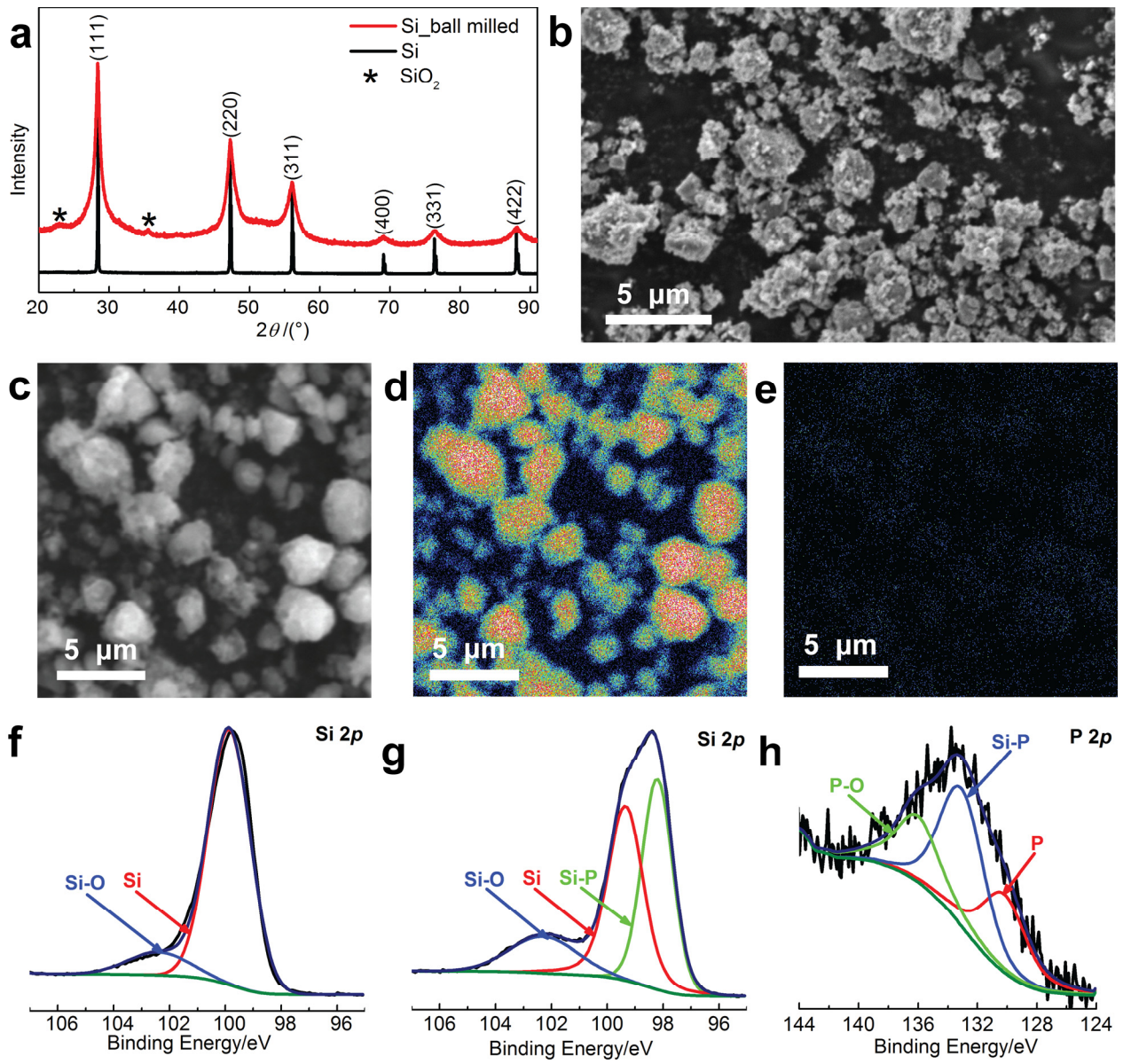

Fig.2 Characterization on the *p*-Si related samples

(a), XRD patterns on the pristine and ball milled Si samples; (b), SEM image of the ball milled Si sample; (c) – (e), SEM-EDX element mapping of the *p*-Si sample: layered image and element mapping of Si and P, respectively. (f), Si 2*p* spectra of the ball milled Si; (g), Si 2*p* and (h), P 2*p* spectra of the *p*-Si sample.

reports the homogeneous distribution of elemental phosphorus next to Si, which indicates a uniform encapsulation of phosphorene on the Si particles.

The Si 2*p* XPS spectrum of ball milled Si (**Fig.2f**) shows a major peak of Si at 99.8 eV and a weak peak at 102.5 eV corresponding to the surface oxidation of Si particles, which is consistent with the XRD analysis; while in the XPS spectrum of the *p*-Si sample (**Fig.2g**), except for the characteristic peak of Si at 99.4 eV, a strong peak is observed at 98.2 eV which can be assigned to the Si–P bond, and a peak at 102.3 eV that can be of allocated to Si–O/Si–O–P. The peaks corresponding to Si and Si–O shift slightly to lower binding energies due to their bonds with phosphorene, which reveals the intimate interactions between the phosphorene encapsulating layer and the Si particles. In addition, Si–O–P bond is also evident in the P 2*p* spectrum of the *p*-Si sample (**Fig.2h**).

The electrochemical performance of the bare Si and the *p*-Si based anodes for Li ion batteries has been characterized within Li ion half-cells. The lithiation capacity of super P carbon black has been determined in our previous work[37] and subtracted from the Si electrode, and the capacity reported in this paper is the capacity calculated based on the mass of Si/*p*-Si. **Fig.3** demonstrates that the *p*-Si based anode achieves an initial reversible capacity of 1577 mAh·g^{-1} for Li ion storage cycling at 0.8 A·g^{-1}, which is relatively lower compared to the bare Si based electrode (1911 mAh·g^{-1}). However, *p*-Si exhibits a much improved cycling stability for

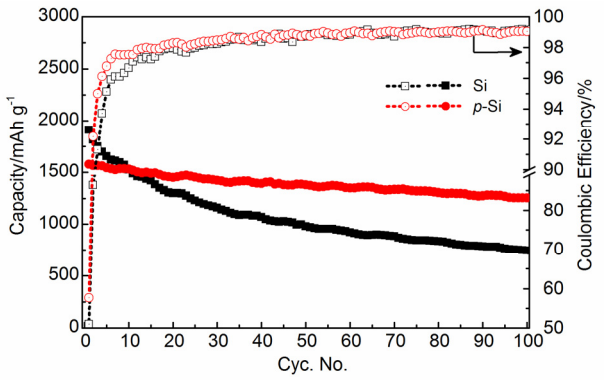

Fig.3 Electrochemical performance

Capacity retentions and Coulombic efficiencies of the Si electrodes with and without phosphorene encapsulation cycling at 0.8 A·g^{-1}.

Li ion uptake compared with the bare Si. The delithiation capacity of the bare Si and *p*-Si amounts to 743 and 1255 mAh·g^{-1}, respectively, in 100 cycles. This can be explained by the observed higher Coulombic efficiency of the *p*-Si anode than bare Si during the initial cycles. The initial coulombic efficiencies amounted to 57.7% and 51.0% for the *p*-Si and bare Si anodes, respectively. Such low initial Coulombic efficiencies originate from the irreversible SEI formation, which mostly occurs during the first cycle. Therefore the Coulombic efficiencies jump to 92.2% and 86.4% for the *p*-Si and Si anodes, respectively, in the 2nd cycle, after which the Coulombic efficiency increases further gradually in both electrodes and *p*-Si shows a higher efficiency than bare Si within the first ~40 cycles.

The low amount (1%) and the semiconductivity of phosphorene in the *p*-Si sample is not expected to change the theoretical capacity or the electrical conductivity of the Si electrode. The significant improvement in capacity retention, Coulombic efficiency and cycling stability upon the addition of phosphorene may result from the following factors: (1), the encapsulating layer of phosphorene may work as a protective layer for Si to confine the volume expansion of Si aggregates and to prevent the material pulverization. (2), the presence of phosphorene on the surface of the Si particles may alter the formation of SEI layer. The phosphorus based SEI layer appears to be thinner and more stable and thus the Coulombic efficiency is enhanced. (3), The strong interactions between phosphorene and Si help to maintain the structural integrity of the electrode facilitating the charge transfer in the electrodes and thus enabling a higher cycling stability. These factors are also consistent with the previous studies [20-24].

When the content of phosphorene increases to 3% and 5% in the *p*-Si sample (**Fig.S1** in the Supporting Information), the capacity of the *p*-Si electrode increases that may be attributed to the facilitated kinetics for Li ion uptake in phosphorene[20]. However, the Coulombic efficiency of the *p*-Si electrode decreases with the increasing amount of phosphorene during the initial ~10 cycles, which may result from the increasing amount of irreversible phosphorene-related SEI formation due to the increasing total surface area of phosphorene nanosheets, and as a result, the cycling stability is compromised.

4 Conclusions

This work reports a facilely synthesized, low-content (1% in mass) phosphorene encapsulated Si based anode, which demonstrates a significantly improved electrochemical performance for reversible Li ion storage over prolonged cycling. This is, to the best of our knowledge, the first introduction of phosphorene encapsulation as a method to suppress the effects of volume expansion and SEI formation, and to promote the cycling stability. Phosphorene encapsulation may thus not only be applied in Si based Li ion anodes, but also may show promise for other high energy density battery materials suffering from substantial volume changes during discharge/charge.

Supporting Information: available free of charge *via* the internet at http://www.whxb.pku.edu.cn.

References

(1) Tarascon, J. M.; Armand, M. *Nature* **2001**, *414*, 359. doi: 10.1038/35104644

(2) Dunn, B.; Kamath, H.; Tarascon, J. M. *Science* **2011**, *334*, 928. doi: 10.1126/science.1212741

(3) Chu, S.; Majumdar, A. *Nature* **2012**, *488*, 294. doi: 10.1038/nature11475

(4) Sun, Y.; Liu, N.; Cui, Y. *Nat. Energy* **2016**, 16071. doi: 10.1038/nenergy.2016.71

(5) Guo, Z. L.; Wu, H. *J. Electrochem.* **2016**, *22*, 499. [郭择良, 伍 晖. 电化学, **2016**, *22,* 499.] doi: 10.13208/j.electrochem.160546

(6) Su, X.; Wu, Q.; Li, J.; Xiao, X.; Lott, A.; Lu, W.; Sheldon, B. W.; Wu, J. *Adv. Energy Mater.* **2014**, *4*, 1300882. doi: 10.1002/aenm.201300882

(7) Wu, H.; Cui, Y. *Nano Today* **2012**, *7*, 414. doi: 10.1016/j.nantod.2012.08.004

(8) Wang, J. T.; Wang, Y.; Huang, B.; Yang, J. Y.; Tan, A.; Lu, S. G. *Acta Phys. -Chim. Sin.* **2014,** *30*, 305. [王建涛, 王 耀, 黄 斌, 杨娟玉, 谭 翱, 卢世刚. 物理化学学报, **2014,** *30*, 305.] doi: 10.3866/PKU.WHXB201312022

(9) Obrovac, M. N.; Christensen, L. *Electrochem. Solid-State Lett.* **2004**, *7*, A93. doi: 10.1149/1.1652421

(10) Pinson, M. B.; Bazant, M. Z. *J. Electrochem. Soc.* **2013**, *160*, A243-A250. doi: 10.1149/2.044302jes

(11) Li, Y.; Yan, K.; Lee, H.-W.; Lu, Z.; Liu, N.; Cui, Y. *Nat. Energy* **2016**,

1, 15029. doi: 10.1038/nenergy.2015.29

(12) Zhou, X.; Yin, Y.-X.; Wan, L.-J.; Guo, Y.-G. *Adv. Energy Mater.* **2012**, *2*, 1086. doi: 10.1002/aenm.201200158

(13) Hu, X.; Jin, Y.; Zhu, B.; Tan, Y.; Zhang, S.; Zong, L.; Lu, Z.; Zhu, J. *ChemNanoMat* **2016**, *2*, 671-674. doi: 10.1002/cnma.201600105

(14) Luo, J.; Zhao, X.; Wu, J.; Jang, H. D.; Kung, H. H.; Huang, J. *J. Phys. Chem. Lett.* **2012**, *3*, 1824. doi: 10.1021/jz3006892

(15) Wen, Y.; Zhu, Y.; Langrock, A.; Manivannan, A.; Ehrman, S. H.; Wang, C. *Small* **2013**, *9*, 2810-2816. doi: 10.1002/smll.201202512

(16) Ling, X.; Wang, H.; Huang, S.; Xia, F.; Dresselhaus, M.S. *Proc. Natl. Acad. Sci. U.S.A.* **2015**, *112*, 4523-4530. doi: 10.1073/pnas.1416581112

(17) Zhang, G.; Huang, S.; Chaves, A.; Song, C.; Özçelik, V. O.; Low, T.; Yan, H. *Nat. Commun.* **2017**, *8*, 14071. doi:10.1038/ncomms14071

(18) Carvalho, A.; Neto, A. H. C. *ACS Cent. Sci.* **2015**, *1*, 289-291. doi: 10.1021/acscentsci.5b00304

(19) Carvalho, A.; Wang, M.; Zhu, X.; Rodin, A. S.; Su, H.; Castro Neto, A. H. *Nat. Rev. Mater.* **2016**, *1*, 16061. doi: 10.1038/natrevmats.2016.61

(20) Congyan, Z.; Ming, Y.; George, A.; Ruchira Ravinath, D.; Gamini, S. *Nanotechnology* **2017**, *28*, 075401. doi: 10.1088/1361-6528/aa52ac

(21) Sun, J.; Lee, H.-W.; Pasta, M.; Yuan, H.; Zheng, G.; Sun, Y.; Li, Y.; Cui, Y. *Nat. Nanotechnol.* **2015**, *10*, 980-985. doi: 10.1038/nnano.2015.194

(22) Arie, A. A.; Lee, J. K., *Mater. Sci. Forum* **2013**, *737*, 80. doi: 10.4028/www.scientific.net/MSF.737.80

(23) Domi, Y.; Usui, H.; Shimizu, M.; Kakimoto, Y.; Sakaguchi, H. *ACS Appl. Mater. Interfaces* **2016**, *8*, 7125. doi: 10.1021/acsami.6b00386

(24) Kim, J. S.; Choi, W.; Byun, D.; Lee, J. K., *Solid State Ion.* **2012**, *212*, 43. doi: 10.1016/j.ssi.2012.01.046

(25) Song, J. O.; Shim, H. T.; Byun, D. J.; Lee, J. K. *Solid State Phenom.* **2007**, *124-126*, 1063. doi: 10.4028/www.scientific.net/SSP.124-126.1063

(26) Yan, C.; Liu, Q.; Gao, J.; Yang, Z.; He, D. *Beilstein J. Nanotechnol.* **2017**, *8*, 222. doi: 10.3762/bjnano.8.24

(27) Brent, J. R.; Savjani, N.; Lewis, E. A.; Haigh, S. J.; Lewis, D. J.; O'Brien, P. *Chem. Commun.* **2014**, *50*, 13338. doi: 10.1039/C4CC05752J

(28) Hernandez, Y., et al., *Nat. Nanotechnol.* **2008**, *3*, 563. doi: 10.1038/nnano.2008.215

(29) Kim, Y.; Park, Y.; Choi, A.; Choi, N.-S.; Kim, J.; Lee, J.; Ryu, J. H.; Oh, S. M.; Lee, K. T. *Adv. Mater.* **2013**, *25*, 3045. doi: 10.1002/adma.201204877

(30) Ramireddy, T.; Xing, T.; Rahman, M. M.; Chen, Y.; Dutercq, Q.; Gunzelmann, D.; Glushenkov, A. M. *J. Mater. Chem. A* **2015**, *3*, 5572. doi: 10.1039/C4TA06186A

(31) Qian, J.; Qiao, D.; Ai, X.; Cao, Y.; Yang, H. *Chem. Commun.* **2012**, *48*, 8931-8933. doi: 10.1039/C2CC34388F

(32) Wang, L.; He, X.; Li, J.; Sun, W.; Gao, J.; Guo, J.; Jiang, C. *Angew. Chem. Int. Ed.* **2012**, *51*, 9034. doi: 10.1002/anie.201204591

(33) Sun, J.; Zheng, G.; Lee, H.-W.; Liu, N.; Wang, H.; Yao, H.; Yang, W.; Cui, Y. *Nano Lett.* **2014**, *14*, 4573. doi: 10.1021/nl501617j

(34) Sun, L. Q.; Li, M. J.; Sun, K.; Yu, S. H.; Wang, R. S.; Xie, H. M. *J. Phys. Chem. C* **2012**, *116*, 14772. doi: 10.1021/jp302265n

(35) Ray, M.; Sarkar, S.; Bandyopadhyay, N. R.; Hossain, S. M.; Pramanick, A. K. *J. Appl. Phys.* **2009**, *105*, 074301. doi: 10.1063/1.3100045

(36) Yim, C.-H.; Courtel, F. M.; Abu-Lebdeh, Y. *J. Mater. Chem. A* **2013**, *1*, 8234-8243. doi: 10.1039/C3TA10883J

(37) Peng, B.; Xu, Y. L.; Wang, X. Q.; Shi, X. H.; Mulder, F. M. *Sci. China-Phys. Mech. Astron.* **2017**, *60*, 064611. doi: 10.1007/s11433-017-9022

Table of Content

Phosphorene encapsulation is for the first time applied to improve the electrochemical performance of Si based Li ion battery anode.

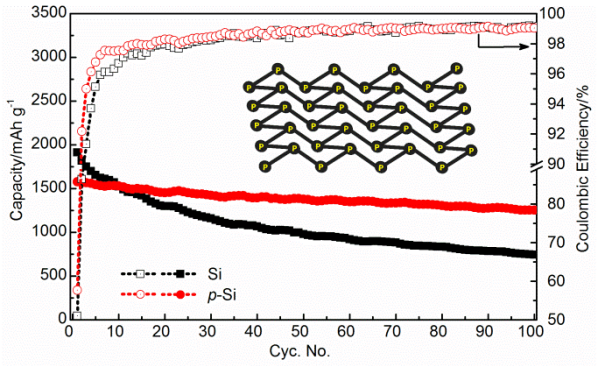

磷烯包覆的高性能硅基锂离子电池负极材料

彭 勃 [1,2]　　徐耀林 [2]　　MULDER Fokko M.[2,*]

([1] 中国人民大学物理系，北京 100872；[2] Materials for Energy Conversion and Storage (MECS), Department of Chemical Engineering, Faculty of Applied Science, Delft University of Technology, Delft 2629 HZ, The Netherlands)

Improving the performance of si-based li-ion battery anodes by utilizing phosphorene encapsulation

PENG Bo[1,2]　　XU Yao-Lin[2]　　MULDER Fokko M.[2,*]

([1]*Department of Physics, Renmin University of China, Beijing 100872, China*; [2]*Materials for Energy Conversion and Storage (MECS), Department of Chemical Engineering, Faculty of Applied Science, Delft University of Technology, Delft 2629 HZ, The Netherlands*)

*Corresponding author. Email: F.M.Mulder@tudelft.nl; Tel: +31-15-2785037

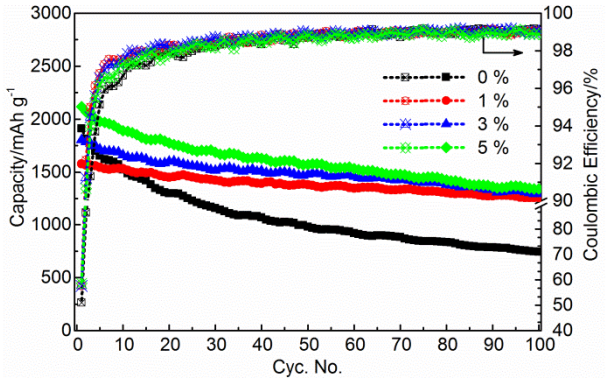

Fig.S1 Electrochemical performance

Capacity retentions and Coulombic efficiencies of the Si electrodes with different amounts of phosphorene in the *p*-Si sample cycling at 0.8 A g^{-1}.